# Performance Bounds on Passive Indoor Positioning using Visible Light

Khaqan Majeed, *Student Member, IEEE,* and Steve Hranilovic, *Senior Member, IEEE*

***Abstract*—In this paper, a novel method for passive indoor localization using LED luminaires is proposed where explicit user participation is not required. This approach measures changes in the impulse response between sources and receivers and estimates a location based on optical channel sounding data. An exponential integrating-sphere model is used to represent object impulse response (OIR) from each luminaire source-receiver pair, which is obtained by subtracting impulse response (IR) of the room background (i.e., without an object) from IR when the object is present inside the room. This model is represented as a function of 3D position of the object and depends on both source and receiver parameters and the physical geometry of the room. An analytical expression of Cramér-Rao lower bound (CRLB) on the proposed passive indoor localization method is derived. The position is also estimated by using a maximum likelihood (ML) estimator which gives the position estimate by maximizing the log-likelihood function of the received noisy OIR waveforms. The results show that the signal-to-noise ratio (SNR) and number of source-receiver pairs used in the estimation play a crucial role in performance. Typical localization root-mean squared error is less than 10 cm over a broad range of light intensities and object locations.**

***Index Terms*—visible light positioning, Cramér-Rao lower bound (CRLB), maximum likelihood (ML) estimator.**

## I. Introduction

INDOOR illumination is dominated by the use of solid-state light-emitting diode (LED) technology due to their energy-efficiency, cost-effectiveness and long life-span. In addition to their primary role as illuminators, the ubiquity of LED luminaires make them suitable to support secondary functions such as indoor communications and positioning. In particular, visible light positioning (VLP) has benefits of leveraging existing illumination installations while providing greater privacy, security and accuracy over comparable radio frequency (RF) approaches. Since light is easily contained by opaque boundaries, VLP emissions are contained to the room of interest which stands in contrast to RF-based positioning where the RF signals travel through walls and are susceptible to eavesdropping. Recent VLP-based techniques [2]–[13] can be broadly categorized into the following categories: proximity-based, received signal strength (RSS)-based and triangulation-based approaches.

In *proximity*-based approaches [8], [14]–[17], the LED light sources are considered to emit a unique signature which is detected by a receiver at the user location. In proximity-based techniques the luminaires are treated as beacons and receivers declare their position based on the closest beacon detected. These techniques typically have low accuracy as compared to other methods [6]. For *RSS*-based techniques [18]–[23] the RSS of received optical signals are used for localization. The average optical power measured at the receiver from several sources is used to estimate receiver location by solving a set of equations which are based on indoor optical wireless channel models (e.g., [24]). A subclass of these methods (e.g., [1], [5], [23]) create a fingerprint map of RSS measurements throughout an indoor space which is constructed during an offline stage. Noisy measurements collected during the online stage are then compared to the stored fingerprint map and the grid point which gives minimum mean squared error between the noisy measurement and stored value in the fingerprint map is returned as the position estimate. These approaches require significant measurements and rely heavily on the accuracy of the underlying models of RSS measurements. *Triangulation*-based techniques [12], [13], [25]–[27] use time-of-arrival (TOA), time-difference-of-arrival (TDOA), or angle-of-arrival (AOA) information from the received optical signals for localization. The time-related information is extracted from the received signals from several sources in TOA and TDOA-based methods, which is then used to solve a set of equations to obtain the position estimate. The AOA-based methods typically employ complex multiple photo-detector (PD) arrays at the receiver to estimate the elevation or azimuth angle of the receiver. Some variants of PD array arrangement have also been studied, for example in [28] a circular PD array for location estimation. The major challenge of these methods is that perfect time synchronization is required between the source and receiver.

In addition to positioning techniques, there has been considerably less work to calculate performance bounds of VLP techniques [27], [29]–[35]. It is common to calculate the Cramér-Rao lower bound (CRLB), which is given as a lower bound on the root mean squared error (RMSE) of an unbiased estimate of unknown variables in mean squared error sense [36]. The CRLB of RSS-based techniques was calculated in [29], [37]. The authors in [30], [31] calculate CRLB for a hybrid RSS/TOA-based technique using multiple PDs at the receiver. The methods in [27], [34] calculate CRLB on TOA-based positioning techniques. All the methods mentioned earlier fall under an *active localization* paradigm, i.e., where the user estimates their position by employing a receiver with a direct line-of-sight (LOS) to the light sources.

This paper presents bounds on the performance of a fundamentally new paradigm in VLP termed *passive localization* [1]. In this approach, light sources and receivers are affixed

K. Majeed and S. Hranilovic are with the Department of Electrical and Computer Engineering, McMaster University, Hamilton, ON, L8S 4L8 Canada e-mail: ({majeedk, hranilovic}@mcmaster.ca).

This work was presented in part at IEEE Globecom 2018 [1].

on the ceiling (potentially co-located) and are controlled by an underlying network (e.g., power-over-ethernet or power line communication channels). Measurements of the impulse responses (IRs) between source-receiver pairs are used to estimate the location of an object in the room. In spite of the challenge of synchronizing amongst sources and receivers, the underlying network can be calibrated to provide a common time reference for measuring IRs as was done in earlier TOA and TDOA work [27], [31], [32], [38]. The measurement of IRs is done such that one source is on at a time and this process is repeated for all the remaining sources. The IR measurements for a given source-receiver pair can be done on the order of 10's of ns and can thus easily be made imperceptible to the human eye. Assuming a single object to be detected in the room, an exponential integrating-sphere model [39], [40] is used to represent the IR of the object to be localized where the parameters of the model depend on the location of the object and the geometry of the room. Using this model, an analytical expression for CRLB is derived as a lower bound on the position estimate error. The position of the object in the room is then estimated using a maximum likelihood (ML) estimator to quantify the performance in a simulation environment. This passive VLP is similar in approach to channel sounding employed in underwater acoustic channels, where measured reflected signals are used to infer position [41] as well as related work in MIMO radar with widely-separated antennas [42]. A related approach has been proposed in parallel in [43], however, they rely only on power measurements for outdoor localization scenarios.

In contrast to existing active VLP approaches, passive VLP does not require fixed beacons, specialized PD arrangements or user involvement in the localization scheme. This passive approach is especially attractive in applications where user involvement in the positioning process is not possible. As an example, consider the need to monitor a patient at home or in a hospital in order to detect an accidental fall while preserving their privacy.

The notation used in this paper are the following: scalar by $x$, constant by $X$, vector by $\mathbf{x}$, $i^{\text{th}}$ element of a vector $\mathbf{x}$ by $x_i$, matrix by $\mathbf{X}$, $i^{\text{th}}$ column of a matrix $\mathbf{X}$ by $\mathbf{x}_i$, $ij^{\text{th}}$ entry of a matrix $\mathbf{X}$ by $x_{ij}$, set by $\mathcal{X}$, set cardinality by $|\mathcal{X}|$, and Euclidean norm of a vector $\mathbf{x}$ by $\|\mathbf{x}\|_2$. Vectors are considered column vectors throughout the paper and $[\cdot]^T$ denotes the transpose operation.

The remainder of the paper is organized as follows. Section II describes the proposed passive localization scenario and the model used to represent IR differences. The analytical expression for CRLB is derived in Section III. The ML position estimation is obtained in Section IV. Numerical results are described and discussed in Section V. Finally, the paper is concluded in Section VI.

## II. System Model

### A. Problem Formulation

Consider an object $o$ inside the room as shown in Figure 1 with $N_s$ light sources and $N_r$ receivers affixed to the ceiling. Though shown to be co-located in Figure 1, which may be the least costly in terms of deployment, sources and receivers can be arbitrarily distributed on the ceiling and are assumed to be parallel to the floor.

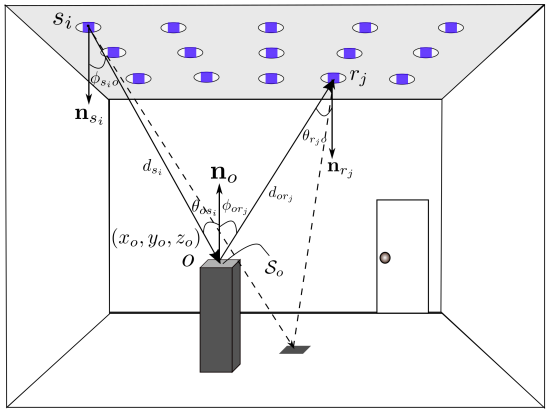


Fig. 1. A room with light sources and receivers affixed on the ceiling. The sources and receivers are co-located. An object (i.e., a cuboid) is also present. A light ray originating from source $s_i$ is reflected from the object (or floor and walls) and received at receiver $r_j$.

The light sources are considered Lambertian emitters [24], [44] with radiation pattern in Watts/steradian

$$R(\phi) = \frac{m+1}{2\pi}(\beta P_s)\cos^m(\phi) \tag{1}$$

where $m$ denotes the Lambertian index of the source, $P_s$ denotes the total power transmitted by the source in Watts, $\beta$ is a factor to control the brightness of the light source, and $\phi$ denotes the angle formed between the normal to the source and a distance vector from source to the object or surface (see Figure 1). Receivers are assumed to have field-of-view (FOV) $\psi$ and effective area $A_r$. Moreover, surfaces of the room and object are modelled as diffuse reflectors.

Consider the example of light rays emerging from source $s_i$ and diffusely reflecting from an object, the floor and walls as shown in Figure 1. The positions of source $s_i$ and receiver $r_j$ are represented by vectors $\mathbf{x}_i^{(s)} = [x_{s_i}\ y_{s_i}\ z_{s_i}]^T$ and $\mathbf{x}_j^{(r)} = [x_{r_j}\ y_{r_j}\ z_{r_j}]^T$ respectively. The object is modelled as a cuboid with a square top denoted by $\mathcal{S}_o$ where $\mathbf{x}_o = [x_o\ y_o\ z_o]^T$ represents the unknown position of the centre of $\mathcal{S}_o$.

Define the *object impulse response* (OIR), $h_{s_i r_j}(t, \mathbf{x}_o)$, as the IR between $s_i$ and $r_j$ considering reflected rays solely from $\mathcal{S}_o$ located at $\mathbf{x}_o$. Using the approach in [44], the OIR can be written as

$$h_{s_i r_j}(t, \mathbf{x}_o) = \sum_{o_k \in \mathcal{S}_o} (\beta P_s) \frac{(m+1)\rho_o A_{r_j} \Delta A_{o_k}}{2\pi d_{s_i o_k}^2 d_{o_k r_j}^2} \cos^m \phi_{s_i o_k} \cos\theta_{o_k s_i} \cos\phi_{o_k r_j} \cos\theta_{r_j o_k} \delta\left(t - \frac{d_{s_i o_k} + d_{o_k r_j}}{c}\right) \tag{2}$$

where $o_k$ is the $k^{\text{th}}$ patch of $\mathcal{S}_o$ so that $\bigcup_k o_k = \mathcal{S}_o$, $\rho_o$ is reflectivity, $A_{r_j}$ is area of the receiver $r_j$, $\Delta A_{o_k}$ is area of $o_k$, and $c$ is the speed of light. In order to compute the OIR in (2), the object surface is discretized into small patches as in [44]. There is a unique path for each ray from source $s_i$ to patch $o_k$ and finally to receiver $r_j$. The OIR in (2) is then the

sum of reflected rays from all the patches on the object's top surface.

In practice, the OIR can be approximated by measurements of the IR between sources and receivers in the room. Let $h_{s_i r_j,e}(t)$ denote the IR of an empty room from $s_i$ to $r_j$ and similarly, $h_{s_i r_j,o}(t,\mathbf{x}_o)$ denotes the IR when the object is present inside the room. Define the *IR difference*, $\bar{h}_{s_i r_j}(t,\mathbf{x}_o)$, as

$$\begin{aligned}\bar{h}_{s_i r_j}(t,\mathbf{x}_o) &= h_{s_i r_j,o}(t,\mathbf{x}_o) - h_{s_i r_j,e}(t) \\ &\approx h_{s_i r_j}(t,\mathbf{x}_o).\end{aligned} \tag{3}$$

In practice the IR differences between source-receiver pairs are taken as an estimate of the OIRs and can be obtained independently and imperceptibly by turning each source-receiver pair on one-at-a-time under the control of an underlying coordination network. The task of the passive localization algorithm is to infer the position $\mathbf{x}_o$ from a collection of IR difference measurements of $\{\bar{h}_{s_i r_j}(t,\mathbf{x}_o)\}$ over $s_i$ and $r_j$.

### B. Comparison of $\bar{h}_{s_i r_j}(t,\mathbf{x}_o)$, $h_{s_i r_j,o}(t,\mathbf{x}_o)$ and $h_{s_i r_j,e}(t)$

The presence of object inside the room modifies the IR. The formation of shadows due to an object $o$ are shown in Figure 2 by considering a single source-receiver pair at a location in an example room scenario. Figure 2a shows two shadows formed on the floor. Shadow $A$ is formed due to obstruction of the light path due to the object top and sides. Shadow $B$, on the other hand, is formed due to shadowing of the receiver because these areas are not visible to the receiver. Figure 2b shows a comparison of IR with and without an object present inside the room, i.e., $h_{s_5 r_6,o}(t,\mathbf{x}_o)$ and $h_{s_5 r_6,e}(t)$. Notice that the presence of an object creates a small peak in IR earlier in time because the top surface of the object is at a shorter distance to the receiver as compared to other surfaces of the object or the room. The difference of two IRs is also shown by a dotted red line. The negative part in the difference corresponds to the shadowing and occurs later in time. An important point to note here is that the red curve is the difference of IRs and not an IR.

In this work only first-order reflections from all surfaces in the room and object are simulated (i.e., light travels from source to receiver through a single reflection). Higher order reflections carry very little power and are often buried in the noise floor of the receiver. Notice also that higher order reflections occur at a later time after the first-order reflections are received and can be easily removed from measured IRs [44]. Thus, for the purposes of passive localization, the IR difference $\bar{h}_{s_i r_j}(t,\mathbf{x}_o)$ is dominated by the first-order reflections from the object surfaces.

### C. Modeling the OIR

Consider modelling the first-order reflections from the object, i.e., the OIR in (2), with the continuous exponential model [39], [40]

$$\tilde{h}_{s_i r_j}(t,\mathbf{x}_o) = \eta_{s_i r_j}(\mathbf{x}_o)\, e^{-\frac{\left(t - t_{s_i r_j}(\mathbf{x}_o)\right)}{\tau_{s_i r_j}(\mathbf{x}_o)}} u_{\sigma_a,\varepsilon}\left(t - t_{s_i r_j}(\mathbf{x}_o)\right) \tag{4}$$

where the parameters $\eta_{s_i r_j}(\mathbf{x}_o)$, $t_{s_i r_j}(\mathbf{x}_o)$ and $\tau_{s_i r_j}(\mathbf{x}_o)$ are related to $\mathbf{x}_o$ in the following. The function $u_{\sigma_a,\varepsilon}(t)$ is the Gaussian cumulative distribution function

$$u_{\sigma_a,\varepsilon}(t) = \frac{1}{2}\left(1 + \operatorname{erf}\left(\frac{t+\varepsilon}{\sqrt{2\sigma_a^2}}\right)\right).$$

The values of $\varepsilon$ and $\sigma_a$ are free parameters chosen to ensure a good fit to the OIR in practice as described in Section V. Notice that for $\varepsilon, \sigma_a \to 0$, that (4) approaches the well-known integrating sphere model for indoor optical intensity impulse responses [40].

The parameters in the OIR model in (4) are a function of unknown position vector $\mathbf{x}_o$, the location of source-receiver pairs, Lambertian parameters of the sources, receiver's parameters, reflectivity of the room surfaces, and the reflectivity of the object surfaces. The distances and angles shown in Figure 1 are defined as

$$\begin{aligned} d_{s_i o} &= \left\|\mathbf{x}_o - \mathbf{x}_i^{(s)}\right\|_2 \\ d_{o r_j} &= \left\|\mathbf{x}_j^{(r)} - \mathbf{x}_o\right\|_2 \\ \phi_{s_i o} &= \theta_{o s_i} = \cos^{-1}\left(\frac{z_{s_i} - z_o}{\left\|\mathbf{x}_o - \mathbf{x}_i^{(s)}\right\|_2}\right) \\ \phi_{o r_j} &= \theta_{r_j o} = \cos^{-1}\left(\frac{z_{r_j} - z_o}{\left\|\mathbf{x}_j^{(r)} - \mathbf{x}_o\right\|_2}\right) \end{aligned} \tag{5}$$

where the angles $\phi_{s_i o}$, $\theta_{o s_i}$, $\phi_{o r_j}$, $\theta_{r_j o}$ are defined with respect to normals $\mathbf{n}_{s_i}$, $\mathbf{n}_o$ and $\mathbf{n}_{r_j}$.

The amplitude parameter $\eta_{s_i r_j}(\mathbf{x}_o)$ in (4) has the same form as the scaling factor in (2) and is related to $\mathbf{x}_o$ as

$$\begin{aligned}\eta_{s_i r_j}(\mathbf{x}_o) = (\beta P_s)\,&\frac{(m+1)\,\rho_o A_{r_j} A_{o,\text{eff}}}{2\pi} \\ &\times \frac{(z_{s_i} - z_o)^{m+1}\left(z_{r_j} - z_o\right)^2}{\left\|\mathbf{x}_o - \mathbf{x}_i^{(s)}\right\|_2^{m+3}\left\|\mathbf{x}_j^{(r)} - \mathbf{x}_o\right\|_2^4}.\end{aligned} \tag{6}$$

The value of $A_{o,\text{eff}}$ is tuned to be a fixed proportion of the area of $\mathcal{S}_o$ in order to have a good fit of $\tilde{h}_{s_i r_j}(t,\mathbf{x}_o)$ to $h_{s_i r_j}(t,\mathbf{x}_o)$ as described in Section V.

The time delay $t_{s_i r_j}(\mathbf{x}_o)$ with respect to the center of $\mathcal{S}_o$ is defined as

$$t_{s_i r_j}(\mathbf{x}_o) = \frac{\left\|\mathbf{x}_o - \mathbf{x}_i^{(s)}\right\|_2}{c} + \frac{\left\|\mathbf{x}_j^{(r)} - \mathbf{x}_o\right\|_2}{c}. \tag{7}$$

This is the total time-of-flight for the signal to travel from $s_i$ to $r_j$ after a first reflection from the object.

The delay spread $\tau_{s_i r_j}(\mathbf{x}_o)$ is a function of $\mathcal{S}_o$ and depends on its orientation with respect to $s_i$ and $r_j$. Consider the top view of $\mathcal{S}_o$ in Figure 3 where the dimensions of $\mathcal{S}_o$ are $2\Delta x \times 2\Delta y$. In this work, the delay spread is estimated as the root mean squared (RMS) value of the delays from the four corners

This article has been accepted for publication in a future issue of this journal, but has not been fully edited. Content may change prior to final publication. Citation information: DOI 10.1109/JLT.2020.2966365, Journal of Lightwave Technology



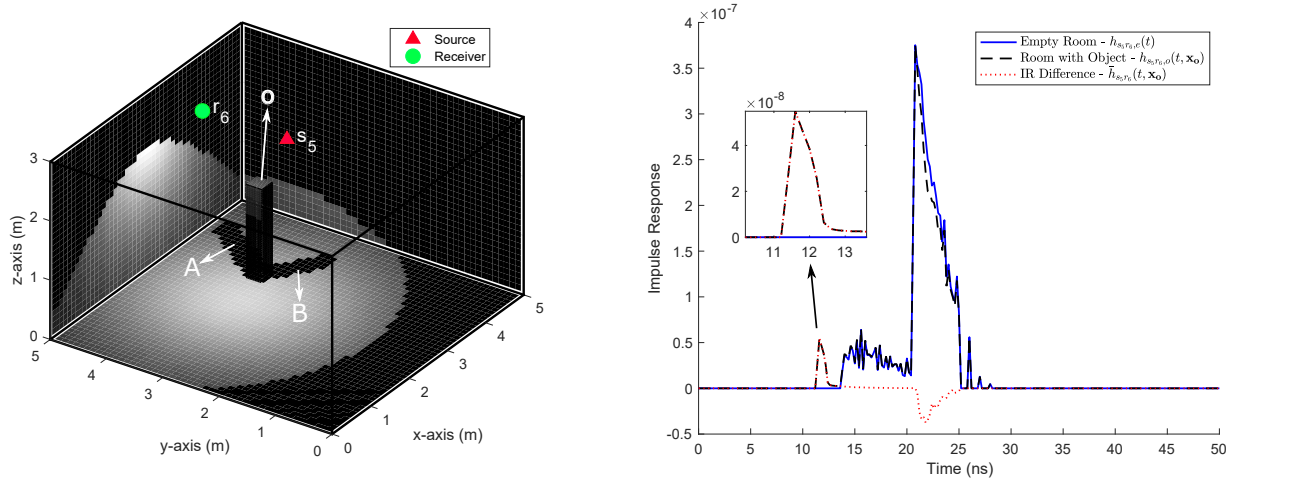


(a) (b)

Fig. 2. The object of fixed height ($z_o = 1.6$ m) is located at $(3.25\,\text{m}, 3.5\,\text{m}, 1.6\,\text{m})$ with all other parameters as defined in Section V. Source $s_5$ and receiver $r_6$ are located at $(2.5\,\text{m}, 2.5\,\text{m}, 3\,\text{m})$ and $(2.5\,\text{m}, 4\,\text{m}, 3\,\text{m})$ respectively: (a) Shadow plot with presence of object and (b) comparison of IR with and without an object inside the room as well as IR difference (first-order reflections considered only).

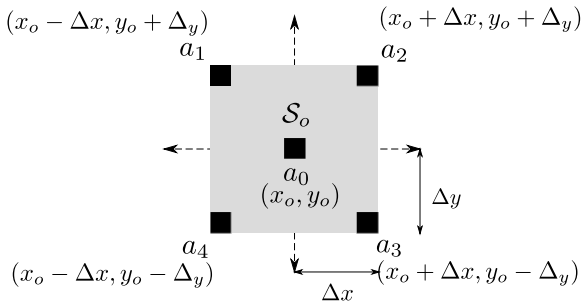


Fig. 3. Top view of the object $\mathcal{S}_o$ showing $x$-$y$ coordinates of its center $a_0$ and corners $a_1$ to $a_4$. The dimensions $2\Delta x \times 2\Delta y$.

of $\mathcal{S}_o$ with respect to the centre at $a_0$. More precisely,

$$\tau_{s_i r_j}(\mathbf{x}_o) = \frac{1}{2} \times \Big( \big(t^{(a_1)}_{s_i r_j}(\mathbf{x}_o) - t_{s_i r_j}(\mathbf{x}_o)\big)^2 + \big(t^{(a_2)}_{s_i r_j}(\mathbf{x}_o) - t_{s_i r_j}(\mathbf{x}_o)\big)^2 + \big(t^{(a_3)}_{s_i r_j}(\mathbf{x}_o) - t_{s_i r_j}(\mathbf{x}_o)\big)^2 + \big(t^{(a_4)}_{s_i r_j}(\mathbf{x}_o) - t_{s_i r_j}(\mathbf{x}_o)\big)^2 \Big)^{\frac{1}{2}} \tag{8}$$

where $t_{s_i r_j}(\mathbf{x}_o)$, $t^{(a_1)}_{s_i r_j}(x_o)$, $t^{(a_2)}_{s_i r_j}(x_o)$, $t^{(a_3)}_{s_i r_j}(x_o)$, and $t^{(a_4)}_{s_i r_j}(x_o)$ denote time delays from the center $a_0$ and corners $a_1$, $a_2$, $a_3$ and $a_4$ of $\mathcal{S}_o$ respectively, as shown in Figure 3.

The expression for $t^{(a_1)}_{s_i r_j}(\mathbf{x}_o)$ is given explicitly in (9) in terms of $\mathbf{x}_o$. The time delays for the other corners can be defined in the similar manner.

### D. Comparison of $h$, $\bar{h}$ and $\tilde{h}$

An example of the OIR, $h_{s_i r_j}(t, \mathbf{x}_o)$, along with the IR difference, $\bar{h}_{s_i r_j}(t, \mathbf{x}_o)$, and model OIR $\tilde{h}_{s_i r_j}(t, \mathbf{x}_o)$ are shown in Figure 4 at a location in a prototypical room (defined in Section V). There is close agreement between the true OIR and the model $\tilde{h}_{s_i r_j}(t, \mathbf{x}_o)$. The estimate of the OIR as measured

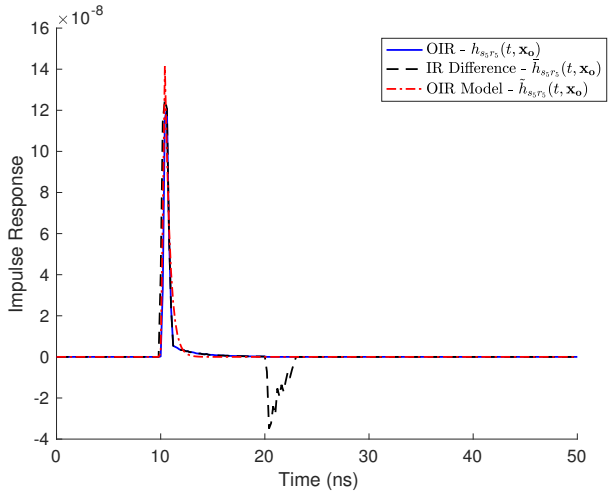


Fig. 4. Simulated OIR (2), IR difference (3) and modelled OIR (4) from source $s_5$ to receiver $r_5$ shown in Figure 5. The object is located at $(3\,\text{m}, 3\,\text{m}, 1.6\,\text{m})$ with all other parameters as defined in Section V.

by the IR difference, $\bar{h}_{s_i r_j}(t, \mathbf{x}_o)$ in (3), also corresponds closely to the OIR, however, has negative amplitudes (at $\approx$ 20 ns) which occur after the reflections from the object (at $\approx$ 10 ns). These negative amplitudes arise in $\bar{h}_{s_i r_j}(t, \mathbf{x}_o)$ since portions of the room are not visible to the receiver due to shadowing of the object as discussed in Section II-B and shown in Figure 2. An important point to emphasize is that $\bar{h}_{s_i r_j}(t, \mathbf{x}_o)$ in (3), is not an IR but rather the difference of IRs with and without the object in the room. As described in Section IV, in practice the negative amplitude shadowing artifacts in $\bar{h}_{s_i r_j}(t, \mathbf{x}_o)$ are clipped at zero to provide a good estimate of the OIR.

$$t_{s_i r_j}^{(a_1)}(\mathbf{x}_o) = \frac{\sqrt{((x_o-\Delta x)-x_{s_i})^2+((y_o+\Delta y)-y_{s_i})^2+(z_o-z_{s_i})^2}}{c} + \frac{\sqrt{\left(x_{r_j}-(x_o-\Delta x)\right)^2+\left(y_{r_j}-(y_o+\Delta y)\right)^2+\left(z_{r_j}-z_o\right)^2}}{c} \quad (9)$$

## III. Cramér-Rao Lower Bound

The CRLB on unbiased estimate $\hat{\mathbf{x}}_o$ of position vector $\mathbf{x}_o$ is derived in this section. The derivation of the bound assumes that the OIR recorded at each receiver has support over the time interval $t = \{0, t_{\max}\}$ typically on the order of 10's of ns. The selection of $t_{\max}$ can be related to the geometry of the room in order to ensure that first-order reflections from the object, which are used to define the OIR in (2), are included. Receivers are assumed to share a common time reference to record the responses emitted from each source. In general, consider that a subset of the measured OIRs are used to estimate position where $\mathcal{D}$ is defined as the collection of $(s_i, r_j)$ pairs used in position estimation. The number of OIR measurements used is a metric of the complexity of the positioning and $\mathcal{D}$ can in practice be selected in many ways (e.g., using $K$ OIRs of highest energy).

The measured OIR from source $s_i$ to receiver $r_j$ can be modelled as

$$z_{s_i r_j}(t) = \tilde{h}_{s_i r_j}(t, \mathbf{x}_o) + n_{s_i r_j}(t) \quad (10)$$

where $n_{s_i r_j}(t)$ is additive white Gaussian noise with zero-mean and variance $\sigma^2$ which is independent of all other source-receiver pairs. Define $\mathcal{Z} = \{z_{s_i,r_j}(t) | (s_i, r_j) \in \mathcal{D}\}$.

The log-likelihood function, considering the model in (10), using a subset of $|\mathcal{D}|$ source-receiver pairs is [36]

$$\Lambda(\mathcal{Z}, \mathbf{x}_o) = C - \sum_{(s_i,r_j)\in\mathcal{D}} \frac{1}{2\sigma^2} \int_0^{t_{\max}} \left(z_{s_i r_j}(t) - \tilde{h}_{s_i r_j}(t, \mathbf{x}_o)\right)^2 dt \quad (11)$$

where $C$ is a constant that does not depend on $\mathbf{x}_o$. Define Fisher information matrix (FIM) $\mathbf{J}(\mathbf{x}_o)$ as

$$\mathbf{J}(\mathbf{x}_o) = E\left\{\left(\nabla_{\mathbf{x}_o}\Lambda(\mathcal{Z}, \mathbf{x}_o)\right)\left(\nabla_{\mathbf{x}_o}\Lambda(\mathcal{Z}, \mathbf{x}_o)\right)^T\right\} \quad (12)$$

where $\nabla_{\mathbf{x}_o}\Lambda(\mathcal{Z}, \mathbf{x}_o)$ is gradient of $\Lambda(\mathcal{Z}, \mathbf{x}_o)$ with respect to $\mathbf{x}_o$ and defined as

$$\nabla_{\mathbf{x}_o}\Lambda(\mathcal{Z}, \mathbf{x}_o) = \left[\begin{array}{ccc} \frac{\partial\Lambda(\mathcal{Z},\mathbf{x}_o)}{\partial x_o} & \frac{\partial\Lambda(\mathcal{Z},\mathbf{x}_o)}{\partial y_o} & \frac{\partial\Lambda(\mathcal{Z},\mathbf{x}_o)}{\partial z_o} \end{array}\right]^T. \quad (13)$$

The CRLB on mean-squared error of the unbiased estimate $\hat{\mathbf{x}}_o$ of $\mathbf{x}_o$ is given as inverse of $\mathbf{J}(\mathbf{x}_o)$ i.e.,

$$E\left\{(\hat{\mathbf{x}}_o - \mathbf{x}_o)(\hat{\mathbf{x}}_o - \mathbf{x}_o)^T\right\} \succeq \mathbf{J}(\mathbf{x}_o)^{-1}. \quad (14)$$

where $\mathbf{M} \succeq \mathbf{N}$ denotes that $(\mathbf{M} - \mathbf{N})$ is positive semi-definite. Given the dimensions of $\mathbf{x}_o$, in order for $\mathbf{J}(\mathbf{x}_o)$ to be invertible OIR measurements from at least three source-receiver pairs are required.

From (11) and (12) the $(k,l)^{\text{th}}$ entry of matrix $\mathbf{J}(\mathbf{x}_o)$ can be expanded as

$$J_{kl}(\mathbf{x}_o) = \sum_{(s_i,r_j)\in\mathcal{D}} \frac{1}{\sigma^2} \int_0^{t_{\max}} \frac{\partial\tilde{h}_{s_i r_j}(t, \mathbf{x}_o)}{\partial \mathbf{x}_{o,k}} \frac{\partial\tilde{h}_{s_i r_j}(t, \mathbf{x}_o)}{\partial \mathbf{x}_{o,l}} dt \quad k, l = 1, 2, 3 \quad (15)$$

The partial derivatives in (15) with respect to $k^{\text{th}}$ element of $\mathbf{x}_o$ can be expanded as shown in (16). Define $\delta_{\sigma_a,\varepsilon}(t) \triangleq \frac{1}{\sigma_a\sqrt{2\pi}} e^{-\frac{(t+\varepsilon)^2}{2\sigma_a^2}}$ as the derivative of $u_{\sigma_a,\varepsilon}(t)$. These partial derivatives are derived in Appendix A.

The CRLB can be computed as

$$\text{CRLB} = \sqrt{\text{tr}\left\{J(\mathbf{x}_o)^{-1}\right\}} \quad (17)$$

where $\text{tr}(\cdot)$ denotes trace of a square matrix, which is a sum of diagonal entries.

## IV. Position Estimation

In an analogous fashion to (10), define the noisy measurement of the OIR between $s_i$ and $r_j$ as

$$\bar{z}_{s_i r_j}(t) = \bar{h}^+_{s_i r_j}(t, \mathbf{x}_o) + n_{s_i r_j}(t) \quad (18)$$

and where $\bar{\mathcal{Z}}$ denotes the collection of such measurements. The signal $\bar{h}^+_{s_i r_j}(t, \mathbf{x}_o)$ is the measured IR difference in (3) where all negative amplitudes are clipped to zero. Define $\hat{\mathbf{x}}_o$ as the ML estimate of $\mathbf{x}_o$ obtained by maximizing the argument of the log-likelihood function $\Lambda\left(\bar{\mathcal{Z}}, \mathbf{x}_o\right)$ defined analogously to (11). Since $C$ and measurements $\bar{\mathcal{Z}}$ do not depend on position, $\Lambda\left(\bar{\mathcal{Z}}, \mathbf{x}_o\right)$ can be simplified as

$$\Lambda\left(\bar{\mathcal{Z}}, \mathbf{x}_o\right) = \sum_{(s_i,r_j)\in\mathcal{D}} \left(\frac{1}{\sigma^2} \int_0^{t_{\max}} \bar{z}_{s_i r_j}(t)\, \tilde{h}_{s_i r_j}(t, \mathbf{x}_o)\, dt - \frac{1}{2\sigma^2} \int_0^{t_{\max}} \tilde{h}^2_{s_i r_j}(t, \mathbf{x}_o)\, dt\right) \quad (19)$$

In practice, the measured IR difference in (18) will be a bandlimited sampled noisy waveform. In the computation of $\hat{\mathbf{x}}_o$, we consider sinc interpolation to relate the samples of $\bar{z}_{s_i r_j}(t)$ to its samples.

$$\frac{\partial \tilde{h}_{s_i r_j}(t, \mathbf{x}_o)}{\partial \mathbf{x}_{o,k}} = -\eta_{s_i r_j}(\mathbf{x}_o) \frac{\partial}{\partial \mathbf{x}_{o,k}} \left\{ t_{s_i r_j}(\mathbf{x}_o) \right\} e^{-\frac{\left(t - t_{s_i r_j}(\mathbf{x}_o)\right)}{\tau_{s_i r_j}(\mathbf{x}_o)}} \delta_{\sigma_a,\varepsilon}\left(t - t_{s_i r_j}(\mathbf{x}_o)\right) + \frac{\partial}{\partial \mathbf{x}_{o,k}} \left\{ \eta_{s_i r_j}(\mathbf{x}_o) e^{-\frac{\left(t - t_{s_i r_j}(\mathbf{x}_o)\right)}{\tau_{s_i r_j}(\mathbf{x}_o)}} \right\} u_{\sigma_a,\varepsilon}\left(t - t_{s_i r_j}(\mathbf{x}_o)\right) \quad \text{for} \quad k = 1, 2, 3 \tag{16}$$

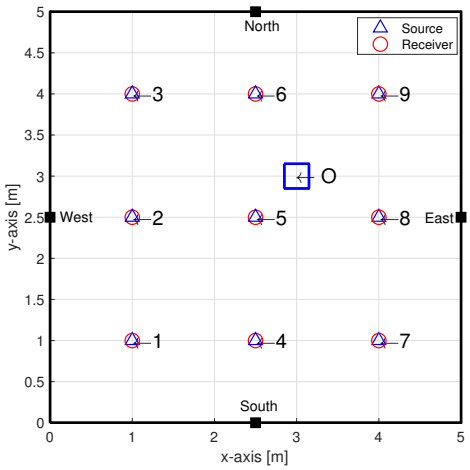


Fig. 5. Top view of the room showing light sources and receivers affixed to the ceiling, which are co-located. The total number of sources and receivers are $N_s = 9$ and $N_r = 9$ respectively. The dimensions of the room are $5\text{m} \times 5\text{m} \times 3\text{m}$. A cuboid object is located at $(3\,\text{m}, 3\,\text{m}, 1.6\,\text{m})$.

The ML estimate $\hat{\mathbf{x}}_o$ is given as

$$\hat{\mathbf{x}}_o = \arg\max_{\mathbf{x}'_o} \sum_{(s_i,r_j)\in\mathcal{D}} \left( \frac{1}{\sigma^2} \int_0^{t_{\max}} \bar{z}_{s_i r_j}(t)\, \tilde{h}_{s_i r_j}(t, \mathbf{x}'_o)\, dt - \frac{1}{2\sigma^2} \int_0^{t_{\max}} \tilde{h}^2_{s_i r_j}(t, \mathbf{x}'_o)\, dt \right). \tag{20}$$

Notice that the CRLB developed in Section III is a lower bound on the positioning performance using the ML estimator (20).

## V. Numerical Results

### A. Simulation Setup

The room considered for simulations is shown in Figure 5 along with an example placement of an object. The values used for several simulation parameters are shown in Table I.

The OIR estimate $\bar{h}_{s_i r_j}(t, \mathbf{x}_o)$ in (3) is simulated by finding $h_{s_i r_j, o}(t, \mathbf{x}_o)$ and $h_{s_i r_j, e}(t)$ using the technique in [44] considering only first-order reflections. The surfaces of room and object are divided into patches of small size, given in Table I, in order to obtain $\bar{h}_{s_i r_j}(t, \mathbf{x}_o)$. Define $\rho_{\text{floor}}$, $\rho_{\text{wall}}$, $\rho_{\text{top}}$, and $\rho_{\text{side}}$ as reflectivity of floor, walls, object's top surface and sides respectively. A value for $A_{o,\text{eff}}$ is found using many trial runs of OIR measurements from different source-receiver pairs and several locations in the room to ensure a good fit with the model.

TABLE I
Simulation Parameters

| | |
|---|---|
| **Room** | Size, $5\,\text{m} \times 5\,\text{m} \times 3\,\text{m}$<br>Patch size, $10\,\text{cm} \times 10\,\text{cm}$<br>No. of sources and receivers, $N_s = 9$, $N_r = 9$<br>Reflection coefficient, $\rho_{\text{floor}} = 0.7$, $\rho_{\text{wall}} = 0.85$<br>Sampling rate of IR, $\Delta t = 0.2$ ns |
| **Light Source** | Transmit power, $P_s = 3$ W<br>Lambertian index, $m = 1$ |
| **Receiver** | FOV (half-angle), $\psi_r = 45\,\text{deg}$<br>Surface area, $A_r = 1\text{cm}^2$<br>Responsivity, $\gamma = 1\text{A/W}$<br>Noise variance, $\sigma^2 = 10^{-16}\text{A}^2$ |
| **Object** | Size, $0.3\,\text{m} \times 0.3\,\text{m} \times 1.6\,\text{m}$<br>Patch size, $3\,\text{cm} \times 3\,\text{cm}$<br>Reflection coefficient, $\rho_{\text{top}} = 0.5$, $\rho_{\text{side}} = 0.6$ |
| **Other parameters** | Gaussian approx. $\epsilon = 0.2$ ns and $\sigma_a^2 = 0.01\text{ns}^2$<br>Object top's effective area, $A_{o,\text{eff}} = 30\%$ of $A_o$ |

The signal-to-noise (SNR) is defined similarly to [45] as

$$\text{SNR} = \frac{\gamma^2 (\beta P_s)^2}{\sigma^2} \tag{21}$$

where $\gamma$ denotes the responsivity of the receiver, which is given in A/W, $P_s$ denotes the total power emitted by a source in Watts, $\beta = \frac{P}{P_s}$ is a factor controlling the total power emitted where $\beta \in \{0.1, 1\}$ i.e., variation from 10% to 100% brightness. The receiver noise has variance $\sigma^2$ and is assumed to be the same for all receivers.

For performance evaluation, the root mean square error (RMSE) between the object's estimated and actual position is obtained for the ML estimate, which is given as

$$\text{RMSE} = \sqrt{(\hat{x}_o - x_o)^2 + (\hat{y}_o - y_o)^2 + (\hat{z}_o - z_o)^2}. \tag{22}$$

The RMSE curves shown in the following subsections are obtained after averaging over several Monte Carlo (MC) runs for each point in the following results.

### B. Variation of luminaire brightness

Figure 6 shows RMSE of the ML estimator plotted against increasing brightness of each source i.e., $\beta$ is varied from 0.1 to 1. As is expected, the performance is poor at low brightness and improves by increasing brightness of the sources. The RMSE curves are also plotted in the figure for a differing

This article has been accepted for publication in a future issue of this journal, but has not been fully edited. Content may change prior to final publication. Citation information: DOI 10.1109/JLT.2020.2966365, Journal of Lightwave Technology



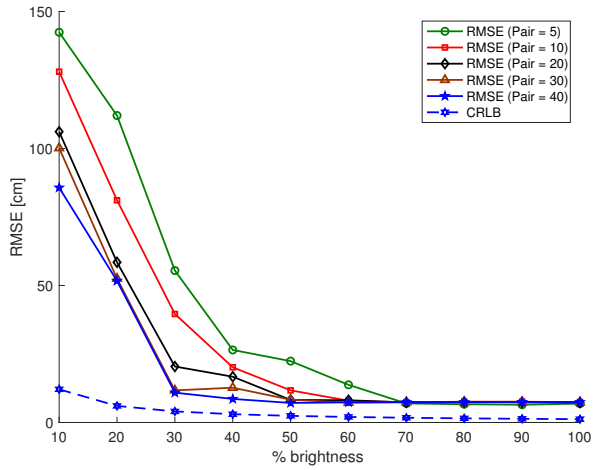


Fig. 6. RMSE against the increasing brightness of sources by considering different number of source-receiver pairs at a time. The object is located at $(3\,\mathrm{m}, 3\,\mathrm{m}, 1.6\,\mathrm{m})$ and RMSE estimated from 100 MC runs.

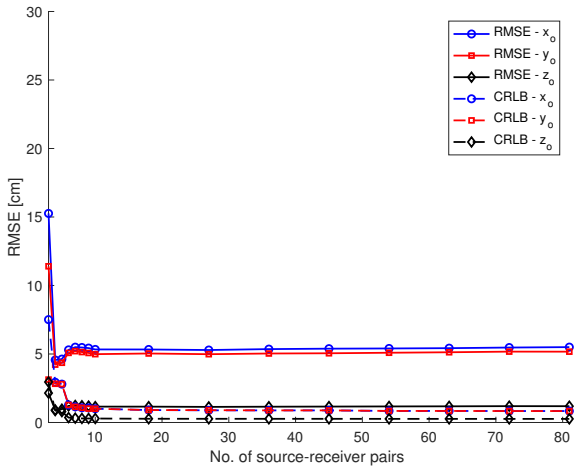


Fig. 8. RMSE and CRLB on RMSE of individual coordinates against the increasing number of source-receiver pairs for the object located at $(3\,\mathrm{m}, 3\,\mathrm{m}, 1.6\,\mathrm{m})$. The number of pairs are varied from 3 to 81, $\beta = 1$ and RMSE results estimated from 20 MC runs.

number of source-receiver pairs, i.e., varying $|\mathcal{D}|$. Notice that better performance is achieved by increasing the number of pairs used at low brightness levels. However, the performance saturates quickly and shows little improvement after a certain number of pairs are used. Additionally, at high brightness, the RMSE also saturates regardless of the number of pairs used. Thus, the same level of performance can be achieved by using a smaller number of pairs at high brightness. This supports the fact that increasing the number of pairs adds up lower energy signals in building up the ML cost function, which do not aid substantially in localization.

The figure also shows a plot of the CRLB from (17) as a lower bound on the RMSE performance. The CRLB curve is obtained by using all source-receiver pairs and varying $\beta$. It should be noted that using all pairs in CRLB evaluation does not imply that all pairs contribute equally to the value of CRLB. This is because some of the receivers can not see the object since it does not fall into receiver's FOV and thus $\bar{h}_{s_i r_j}(t, \mathbf{x}_o)$ consists only of noise.

### C. Variation of number of source-receiver pairs

Figure 7 shows contour plots of the RMSE and CRLB against the increasing brightness of sources and number of source-receiver pairs used in estimation. From Figure 7a, while the RMSE is improved both by increasing the brightness of the sources and number of pairs measured, the performance is most sensitive to the choice of $\beta$. For example, at low brightness the performance is little improved even after including a considerable number of pairs. At high brightness and using a large number of measured pairs the performance, both in terms of RMSE and CRLB, becomes saturated. It is observed that the performance of the positioning algorithm is typically dominated by few high energy measured pairs which have a small time-of-flight from the corresponding sources to receivers.

### D. CRLB on RMSE of individual coordinates

The RMSE and CRLB on individual coordinates is evaluated by increasing the number of source-receiver pairs. Figure 8 shows plots of RMSE and CRLB on RMSE of individual coordinates. The number of pairs are varied from 3 to all possible (81 in this case). Notice that the results in $x$ an $y$ axes largely mirror one another as is expected. Additionally, notice that the positioning estimation for $z$-coordinate is more accurate than the other coordinates. This is consistent with the fact that the Lambertian model has uniaxial symmetry in the $x$-$y$ plane as compared to the $z$-axis and thus adds more uncertainty in the $x$-$y$ plane. The positioning performance saturates with increasing numbers of pairs since the addition of low energy pairs does not contribute much to performance improvement.

### E. CRLB variation over the room

The CRLB over a spatial grid is evaluated by moving an object of fixed height across the room. All the source-receiver pairs are used to evaluate CRLB. The discretization is done along $x$ and $y$ axes at a resolution of 10 cm and the CRLB is computed at each point. Figure 9 presents contour plots of CRLB by using different brightness levels of sources i.e., varying $\beta$. It can be observed from the plots that the CRLB is improved by increasing the brightness in room. This is expected because changing brightness of the sources means changing SNR of the received OIR. Notice also that the CRLB is the highest along edges of the room. This is because when the object is around those locations then only a few source-receiver pairs are visible and able to contribute to the positioning estimate. It is also observed that the CRLB has small fluctuations within the space between the luminaires and the receivers. This effect is most prominent at low dimming levels, i.e., $\beta = 0.25$, and is largely due to the fact that limited FOV of the receivers excludes certain pairs from the position estimate.

This article has been accepted for publication in a future issue of this journal, but has not been fully edited. Content may change prior to final publication. Citation information: DOI 10.1109/JLT.2020.2966365, Journal of Lightwave Technology



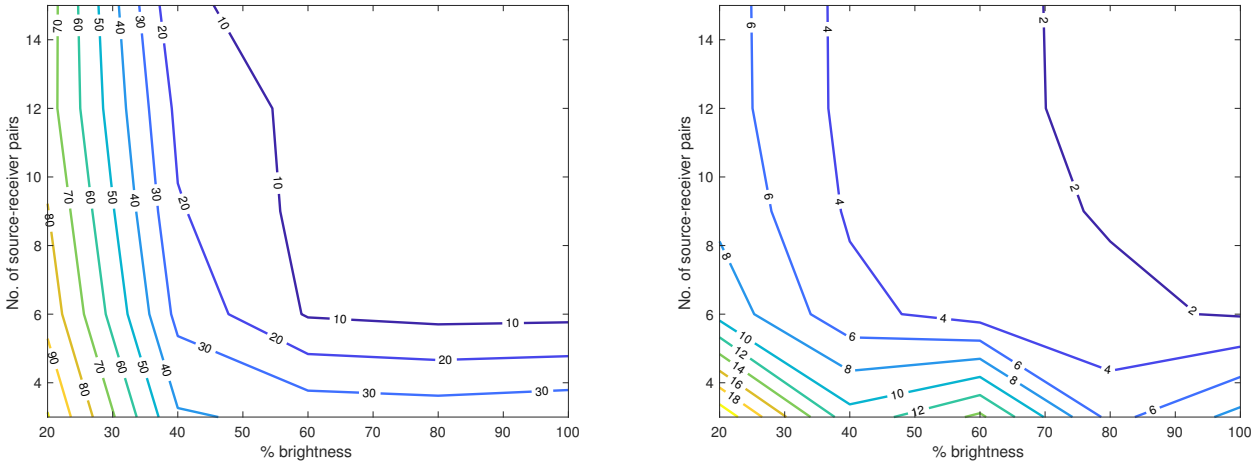


(a) (b)

Fig. 7. Contour plots of performance against source brightness and the number of OIR measurement pairs for the case of an object located at $(3\,\mathrm{m}, 3\,\mathrm{m}, 1.6\,\mathrm{m})$: (a) RMSE [cm] (estimated from 50 MC runs.), (b) CRLB [cm].

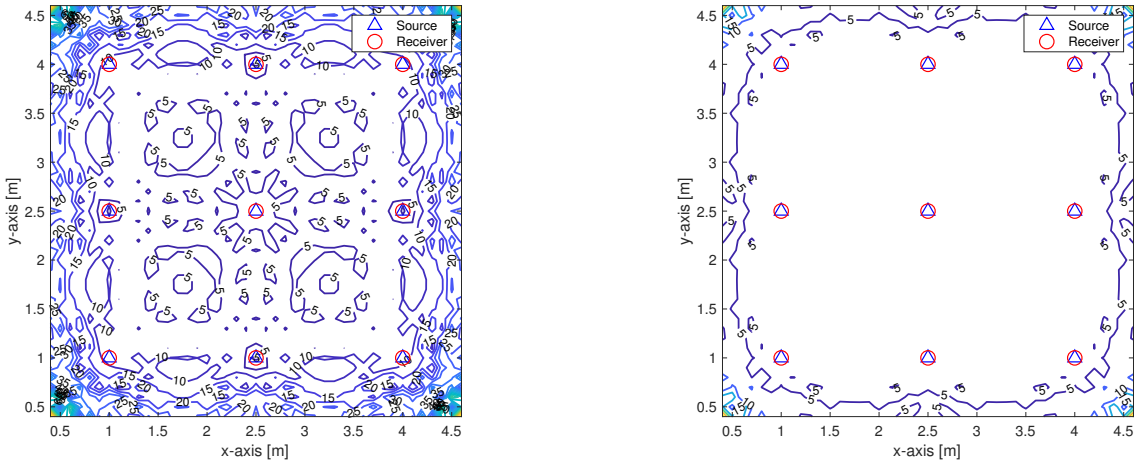


(a) (b)

Fig. 9. Contour plots of CRLB [cm] against spatial variation in the room for an object of fixed height ($z_o = 1.6$ m) for (a) $\beta = 0.25$, (b) $\beta = 1$.

## VI. Conclusions

Passive indoor positioning using luminaires and receivers in a room is proposed where positioning estimates are derived using reflected energy from an object in the room. Unlike earlier active positioning approaches, our passive positioning approach does not require direct user intervention.

In particular, we model the reflected object impulse response (OIR) between different source-receiver pairs using exponential-integrating sphere model. The model is represented as a function of the object's position as well as source and receiver parameters, and the physical geometry of the room. The OIR measurements can be obtained from each source-receiver pair in a short interval of time by using a coordinating backbone network. Both an ML estimator as well as an analytical CRLB expression are derived.

The results show that performance is improved both by increasing the number of collected source-receiver signals as well as the brightness of the luminaires. Positioning performance is shown to be most sensitive to the dimming level which controls the overall SNR of the system. The performance is also improved by increasing the number of source-receiver pairs measured, however, it saturates quickly. This is consistent with the fact that performance is dominated by several high energy source-receiver pairs. Thus, at high brightness satisfactory performance can be obtained with less complexity by choosing the optimum number of OIR measurements to use in the estimation. When the user dims the lights, similar performance is possible, at greater complexity, by collecting more OIR measurements from a greater number of source-receiver pairs. With typical in room parameters, RMSE of less that 10 cm was found both through simulation and in the developed lower bounds on positioning performance.

Future work includes extending the formulation to consider multiple objects in the room. In addition, the impact of tilt and misalignment in the sources and receivers as well as synchronization errors will also be considered in the future to reflect realistic physical impairments.

## APPENDIX A
## PARTIAL DERIVATIVES

The partial derivatives needed to compute the CRLB given in Section III are rather involved and the procedure to obtain them is described in this appendix. The partial derivative in the first term of (16) with respect to $x_o$ is given as

$$\frac{\partial}{\partial x_o}\left\{t_{s_i r_j}\left(\mathbf{x}_o\right)\right\} = \left(\frac{x_o - x_{s_i}}{c\left\|\mathbf{x}_o - \mathbf{x}_i^{(s)}\right\|_2} - \frac{x_{r_j} - x_o}{c\left\|\mathbf{x}_j^{(r)} - \mathbf{x}_o\right\|_2}\right). \tag{23}$$

The derivative of the second term in (16) can be expanded using the product rule of derivatives as shown in (24). The partial derivative of $\tau_{s_i r_j}\left(\mathbf{x}_o\right)$ in (24) can be further expanded as shown in (25). As an example, (26) presents the partial derivative of time delay from corner $a_1$ of $\mathcal{S}_o$ elaborated in Figure 3. The derivatives for other corners can be derived in the similar manner. The partial derivatives with respect to $y_o$ can be derived in the same fashion since there exists symmetry in $x$ and $y$ coordinates.

Consider the partial derivative with respect to $z_o$ in (16) (i.e., $k = 3$). The partial derivative in first term of (16) with respect to $z_o$ is similar to (23). The partial derivative of second term of (16) with respect to $z_o$ can be expanded similarly using the product rule of derivatives and is given in (27). The partial derivative $\tau_{s_i r_j}\left(\mathbf{x}_o\right)$ with respect to $z_o$ can be expanded in a similar fashion to (25). As was done for $x$ and $y$ coordinates, the partial derivative of time delay from corner $a_1$ of the object top with respect to $z_o$ is given in (28). The partial derivatives for other corners can be derived similarly.

## ACKNOWLEDGMENT

The authors would like to thank Drs. R. Tharmarasa and T.N. Davidson for their helpful discussions in the formulation of this work.

## REFERENCES

[1] K. Majeed and S. Hranilovic, "Passive Indoor Localization for Visible Light Communication Systems," *2018 IEEE Glob. Commun. Conf.*, pp. 1–6, 2019.

[2] Q. Xu, R. Zheng, and S. Hranilovic, "IDyLL: Indoor Localization using Inertial and Light Sensors on Smartphones," in *Proc. ACM Int. Jt. Conf. Pervasive Ubiquitous Comput. UbiComp 2015*, no. SEPTEMBER 2015, 2015, pp. 307–318.

[3] Z. Zhou, M. Kavehrad, and P. Deng, "Indoor positioning algorithm using light-emitting diode visible light communications," *Opt. Eng.*, vol. 51, no. 8, p. 085009, 2012.

[4] Y.-s. Kuo, P. Pannuto, K.-j. Hsiao, P. Dutta, and A. Arbor, "Luxapose : Indoor Positioning with Mobile Phones and Visible Light," in *Mobicom'14*, 2014, pp. 299–301.

[5] H. Hosseinianfar, M. Noshad, and M. Brandt-Pearce, "Positioning for visible light communication system exploiting multipath reflections," *IEEE Int. Conf. Commun.*, 2017.

[6] J. Armstrong, Y. Sekercioglu Ahmet, and A. Neild, "Visible light positioning: A roadmap for international standardization," *IEEE Commun. Mag.*, vol. 51, no. 12, pp. 68–73, 2013.

[7] S. H. Madoka Nakajima, "Indoor navigation system for visually impaired people using visible light communication and compensated geomagnetic sensing," in *IEEE Int. Conf. Commun. China Wirel. Commun. Syst.*, 2012, pp. 524–529.

[8] H. S. Liu and G. Pang, "Positioning Beacon System Using Digital Camera and LEDs," *IEEE Trans. Veh. Technol.*, vol. 52, no. 2, pp. 406–419, 2003.

[9] X. Liu, H. Makino, S. Kobayashi, and Y. Maeda, "Design of an indoor self-positioning system for the visually impaired - Simulation with RFID and bluetooth in a visible light communication system -," in *Annu. Int. Conf. IEEE Eng. Med. Biol. - Proc.*, vol. 4, no. 3, 2007, pp. 1655–1658.

[10] L. Li, P. Hu, C. Peng, G. Shen, and F. Zhao, "Epsilon: A Visible Light Based Positioning System," in *USENIX Symp. Netw. Syst. Des. Implement.*, no. 1, 2014, pp. 331–343.

[11] H. S. Kim, D. R. Kim, S. H. Yang, Y. H. Son, and S. K. Han, "An indoor visible light communication positioning system using a RF carrier allocation technique," *J. Light. Technol.*, vol. 31, no. 1, pp. 134–144, 2013.

[12] T. H. Do, J. Hwang, and M. Yoo, "TDoA based indoor visible light positioning systems," in *Int. Conf. Ubiquitous Futur. Networks, ICUFN*, 2013, pp. 456–458.

[13] U. Nadeem, N. Hassan, M. Pasha, and C. Yuen, "Highly accurate 3D wireless indoor positioning system using white LED lights," *Electron. Lett.*, vol. 50, no. 11, pp. 828–830, 2014.

[14] G. K. H. Pang and H. H. S. Liu, "LED Location Beacon System Based on Processing of Digital Images," *IEEE Trans. Intell. Transp. Syst.*, vol. 2, no. 3, pp. 135–150, 2001.

[15] M. Nakajima and S. Haruyama, "New indoor navigation system for visually impaired people using visible light communication," *EURASIP J. Wirel. Commun. Netw.*, vol. 2013, no. 1, p. 37, 2013.

[16] C. Sertthin, E. Tsuji, M. Nakagawa, S. Kuwano, and K. Watanabe, "A switching estimated receiver position scheme for visible light based indoor positioning system," in *2009 4th Int. Symp. Wirel. Pervasive Comput. ISWPC 2009*, 2009.

[17] G. Del Campo-Jimenez, J. M. Perandones, and F. J. Lopez-Hernandez, "A VLC-based beacon location system for mobile applications," in *2013 Int. Conf. Localization GNSS, ICL-GNSS 2013*, no. Id, 2013, pp. 3–6.

[18] S.-K. Han, Y.-Y. Won, D.-H. Kim, and S.-H. Yang, "Three-dimensional optical wireless indoor positioning system using location code map based on power distribution of visible light emitting diode," *IET Optoelectron.*, vol. 7, no. 3, pp. 77–83, 2013.

[19] P. Luo, M. Zhang, X. Zhang, G. Cai, D. Han, and Q. Li, "An Indoor Visible Light Communication Positioning System Using Dual-Tone Multi-Frequency Technique," in *Int. Work. Opt. Wirel. Commun.*, 2013, pp. 25–29.

[20] S.-K. Han, E.-M. Jeong, D.-R. Kim, Y.-H. Son, S.-H. Yang, and H.-S. Kim, "Indoor three-dimensional location estimation based on LED visible light communication," *Electron. Lett.*, vol. 49, no. 1, pp. 54–56, 2013.

[21] S.-Y. Jung, S. R. Lee, and C.-S. Park, "Indoor location awareness based on received signal strength ratio and time division multiplexing using light-emitting diode light," *Opt. Eng.*, vol. 53, no. 1, p. 016106, 2014.

[22] W. Gu, M. Aminikashani, P. Deng, and M. Kavehrad, "Impact of Multipath Reflections on the Performance of Indoor Visible Light Positioning Systems," *J. Light. Technol.*, vol. 34, no. 10, pp. 2578–2587, 2016.

[23] A. Danideh and R. A. Sadeghzadeh, "CPW-fed slot antenna for MIMO system applications," *Indian J. Sci. Technol.*, vol. 6, no. 1, pp. 3872–3875, 2013.

[24] J. M. Kahn and J. R. Barry, "Wireless Infrared Communications," *Proc. IEEE*, vol. 9219, no. 97, pp. 265–298, 1997.

[25] J. H. Y. Nah, R. Parthiban, and M. H. Jaward, "Visible light communications localization using TDOA-based coherent heterodyne detection," in *4th Int. Conf. Photonics, ICP 2013 - Conf. Proceeding*, 2013, pp. 247–249.

[26] S. Y. Jung, S. Hann, and C. S. Park, "TDOA-based optical wireless indoor localization using LED ceiling lamps," *IEEE Trans. Consum. Electron.*, vol. 57, no. 4, pp. 1592–1597, 2011.

[27] T. Q. Wang, Y. A. Sekercioglu, A. Neild, and J. Armstrong, "Position accuracy of time-of-arrival based ranging using visible light with application in indoor localization systems," *J. Light. Technol.*, vol. 31, no. 20, pp. 3302–3308, 2013.

[28] S. Lee and S. Y. Jung, "Location awareness using Angle-of-arrival based circular-PD-array for visible light communication," in *APCC 2012 - 18th Asia-Pacific Conf. Commun. "Green Smart Commun. IT Innov.*, 2012, pp. 480–485.

$$\frac{\partial}{\partial x_o}\left\{\eta_{s_ir_j}\left(\mathbf{x}_o\right)e^{-\frac{\left(t-t_{s_ir_j}(\mathbf{x}_o)\right)}{\tau_{s_ir_j}(\mathbf{x}_o)}}\right\}=\eta_{s_ir_j}\left(\mathbf{x}_o\right)e^{-\frac{\left(t-t_{s_ir_j}(\mathbf{x}_o)\right)}{\tau_{s_ir_j}(\mathbf{x}_o)}}\left(\frac{\tau_{s_ir_j}\left(\mathbf{x}_o\right)\frac{\partial t_{s_ir_j}(\mathbf{x}_o)}{\partial x_o}-\left(t_{s_ir_j}\left(\mathbf{x}_o\right)-t\right)\frac{\partial \tau_{s_ir_j}(\mathbf{x}_o)}{\partial x_o}}{\left(\tau_{s_ir_j}\left(\mathbf{x}_o\right)\right)^2}\right)$$
$$+\eta_{s_ir_j}\left(\mathbf{x}_o\right)e^{-\frac{\left(t-t_{s_ir_j}(\mathbf{x}_o)\right)}{\tau_{s_ir_j}(\mathbf{x}_o)}}\left(\frac{4\left(x_{r_j}-x_o\right)}{\left\|\mathbf{x}_j^{(r)}-\mathbf{x}_o\right\|_2^2}-\frac{(m+3)\left(x_o-x_{s_i}\right)}{\left\|\mathbf{x}_o-\mathbf{x}_i^{(s)}\right\|_2^2}\right) \tag{24}$$

$$\frac{\partial \tau_{s_ir_j}\left(\mathbf{x}_o\right)}{\partial x_o}=\frac{1}{4\tau_{s_ir_j}\left(\mathbf{x}_o\right)}$$
$$\times\left\{\left(t_{s_ir_j}^{(a_1)}\left(\mathbf{x}_o\right)-t_{s_ir_j}\left(\mathbf{x}_o\right)\right)\left(\frac{\partial t_{s_ir_j}^{(a_1)}\left(\mathbf{x}_o\right)}{\partial x_o}-\frac{\partial t_{s_ir_j}\left(\mathbf{x}_o\right)}{\partial x_o}\right)+\left(t_{s_ir_j}^{(a_2)}\left(\mathbf{x}_o\right)-t_{s_ir_j}\left(\mathbf{x}_o\right)\right)\left(\frac{\partial t_{s_ir_j}^{(a_2)}\left(\mathbf{x}_o\right)}{\partial x_o}-\frac{\partial t_{s_ir_j}\left(\mathbf{x}_o\right)}{\partial x_o}\right)\right.$$
$$\left.+\left(t_{s_ir_j}^{(a_3)}\left(\mathbf{x}_o\right)-t_{s_ir_j}\left(\mathbf{x}_o\right)\right)\left(\frac{\partial t_{s_ir_j}^{(a_3)}\left(\mathbf{x}_o\right)}{\partial x_o}-\frac{\partial t_{s_ir_j}\left(\mathbf{x}_o\right)}{\partial x_o}\right)+\left(t_{s_ir_j}^{(a_4)}\left(\mathbf{x}_o\right)-t_{s_ir_j}\left(\mathbf{x}_o\right)\right)\left(\frac{\partial t_{s_ir_j}^{(a_4)}\left(\mathbf{x}_o\right)}{\partial x_o}-\frac{\partial t_{s_ir_j}\left(\mathbf{x}_o\right)}{\partial x_o}\right)\right\} \tag{25}$$

$$\frac{\partial t_{s_ir_j}^{(a_1)}\left(\mathbf{x}_o\right)}{\partial x_o}=\frac{c^{-1}\left(\left(x_o-\Delta x\right)-x_{s_i}\right)}{\sqrt{\left(\left(x_o-\Delta x\right)-x_{s_i}\right)^2+\left(\left(y_o+\Delta y\right)-y_{s_i}\right)^2+\left(z_o-z_{s_i}\right)^2}}$$
$$-\frac{c^{-1}\left(x_{r_j}-\left(x_o-\Delta x\right)\right)}{\sqrt{\left(x_{r_j}-\left(x_o-\Delta x\right)\right)^2+\left(y_{r_j}-\left(y_o+\Delta y\right)\right)^2+\left(z_{r_j}-z_o\right)^2}} \tag{26}$$

$$\frac{\partial}{\partial z_o}\left\{\eta_{s_ir_j}\left(\mathbf{x}_o\right)e^{-\frac{\left(t-t_{s_ir_j}(\mathbf{x}_o)\right)}{\tau_{s_ir_j}(\mathbf{x}_o)}}\right\}=\eta_{s_ir_j}\left(\mathbf{x}_o\right)e^{-\frac{\left(t-t_{s_ir_j}(\mathbf{x}_o)\right)}{\tau_{s_ir_j}(\mathbf{x}_o)}}\left(\frac{\tau_{s_ir_j}\left(\mathbf{x}_o\right)\frac{\partial t_{s_ir_j}(\mathbf{x}_o)}{\partial z_o}-\left(t_{s_ir_j}\left(\mathbf{x}_o\right)-t\right)\frac{\partial \tau_{s_ir_j}(\mathbf{x}_o)}{\partial z_o}}{\left(\tau_{s_ir_j}\left(\mathbf{x}_o\right)\right)^2}\right)$$
$$+\eta_{s_ir_j}\left(\mathbf{x}_o\right)e^{-\frac{\left(t-t_{s_ir_j}(\mathbf{x}_o)\right)}{\tau_{s_ir_j}(\mathbf{x}_o)}}\left(-\frac{2}{z_{r_j}-z_o}-\frac{(m+1)}{z_{s_i}-z_o}+\frac{4\left(z_{r_j}-z_o\right)}{\left\|\mathbf{x}_j^{(r)}-\mathbf{x}_o\right\|_2^2}-\frac{(m+3)\left(z_o-z_{s_i}\right)}{\left\|\mathbf{x}_o-\mathbf{x}_i^{(s)}\right\|_2^2}\right) \tag{27}$$

$$\frac{\partial t_{s_ir_j}^{(a_1)}\left(\mathbf{x}_o\right)}{\partial z_o}=\frac{c^{-1}\left(z_o-z_{s_i}\right)}{\sqrt{\left(\left(x_o-\Delta x\right)-x_{s_i}\right)^2+\left(\left(y_o+\Delta y\right)-y_{s_i}\right)^2+\left(z_o-z_{s_i}\right)^2}}$$
$$-\frac{c^{-1}\left(z_{r_j}-z_o\right)}{\sqrt{\left(x_{r_j}-\left(x_o-\Delta x\right)\right)^2+\left(y_{r_j}-\left(y_o+\Delta y\right)\right)^2+\left(z_{r_j}-z_o\right)^2}} \tag{28}$$


[29] X. Zhang, J. Duan, Y. Fu, and A. Shi, "Theoretical accuracy analysis of indoor visible light communication positioning system based on received signal strength indicator," *J. Light. Technol.*, vol. 32, no. 21, pp. 3578–3584, 2014.

[30] H. Steendam, T. Q. Wang, and J. Armstrong, "Theoretical lower bound for indoor visible light positioning using received signal strength measurements and an aperture-based receiver," *J. Light. Technol.*, vol. 35, no. 2, pp. 309–319, 2017.

[31] M. F. Keskin and S. Gezici, "Comparative Theoretical Analysis of Distance Estimation in Visible Light Positioning Systems," *J. Light. Technol.*, vol. 34, no. 3, pp. 854–865, 2016.

[32] M. F. Keskin, S. Gezici, and O. Arikan, "Direct positioning in synchronous and asynchronous visible light systems," *IEEE Trans. Commun.*, vol. 66, no. 1, pp. 239–254, 2018.

[33] E. Gonendik and S. Gezici, "Fundamental limits on RSS based range estimation in visible light positioning systems," *IEEE Commun. Lett.*, vol. 19, no. 12, pp. 2138–2141, 2015.

[34] C. Amini, A. Taherpour, T. Khattab, and S. Gazor, "Theoretical accuracy analysis of indoor visible light communication positioning system based on time-of-arrival," *Can. Conf. Electr. Comput. Eng.*, vol. 2016-Octob, pp. 1–5, 2016.

[35] N. Stevens and H. Steendam, "Magnitude of the Distance Estimation Bias in Received Signal Strength Visible Light Positioning," *IEEE Commun. Lett.*, vol. 22, no. 11, pp. 2250–2253, 2018.

[36] H. L. V. Trees, *Detection, Estimation, and Modulation Theory, Part I*. John Wiley & Sons, Inc., 2001.

[37] Z. Zheng, L. Liu, and W. Hu, "Accuracy of Ranging Based on DMT Visible Light Communication for Indoor Positioning," *IEEE Photonics Technol. Lett.*, vol. 29, no. 8, pp. 679–682, 2017.

[38] T.-H. Do and M. Yoo, "TDOA-based indoor positioning using visible light," *Photonic Netw. Commun.*, vol. 27, no. 2, pp. 80–88, 2014.

[39] V. Jungnickel, V. Pohl, S. Nönnig, and C. von Helmolt, "A physical model of the wireless infrared communication channel," *IEEE J. Sel. Areas Commun.*, vol. 20, no. 3, pp. 631–640, 2002.

[40] V. Pohl, V. Jungnickel, and C. Helmolt, "Integrating-sphere diffuser for wireless infrared communication," in *IEE Proc. - Optoelectron.*, vol. 147, no. 4, 2000, pp. 281–285.

[41] J. Rudander, T. Husoy, and P. V. Walree, "Shallow-Water Channel Sounding for High Speed Acoustic Communication," in *Ocean. 2017 - Aberdeen*, 2017, pp. 1–8.

[42] M. S. Davis, G. A. Showman, and A. D. Lanterman, "Coherent MIMO radar: The phased array and orthogonal waveforms," *IEEE Aerosp. Electron. Syst. Mag.*, vol. 29, no. 8, pp. 76–91, 2014.
[43] W. Wang, J. Zhang, Q. Wang, and M. Zuniga, "Leveraging smart lights for passive localization," *Proc. - 15th IEEE Int. Conf. Mob. Ad Hoc Sens. Syst. MASS 2018*, no. Section IV, pp. 272–280, 2018.
[44] J. R. Barry, J. M. Kahn, W. J. Krause, E. A. Lee, and D. G. Messerschmitt, "Simulation of Multipath Impulse Response for Indoor Wireless Optical Channels," *IEEE J. Sel. Areas Commun.*, vol. 11, no. 3, pp. 367–379, 1993.
[45] J. Grubor, S. Randel, K. D. Langer, and J. W. Walewski, "Broadband information broadcasting using LED-based interior lighting," *J. Light. Technol.*, vol. 26, no. 24, pp. 3883–3892, 2008.

**Khaqan Majeed (S'15)** is a PhD candidate in the Department of Electrical and Computer Engineering at McMaster University. He received his MS degree in electrical engineering from King Fahd University of Petroleum and Minerals (KFUPM), Dhahran, Saudi Arabia in 2014 and B.Sc. degree (first division with honours) in electrical engineering from University of Engineering and Technology (UET) Lahore, Pakistan in 2009. Previously, he was a Lab Instructor in the Department of Electrical Engineering, Prince Mohammad Bin Fahd University (PMU), Al-Khobar, Saudi Arabia from Sep, 2014 to May, 2016. He also served as a lab engineer cum lecturer in the Department of Electrical Engineering, University of Management and Technology (UMT), Lahore, Pakistan from Oct, 2009 to Apr, 2011. His research interests lie in the areas of indoor localization, visible light positioning (VLP), and machine learning.

**Steve Hranilovic (S'94-M'03-SM'07)** received the B.A.Sc. degree with honours in electrical engineering from the University of Waterloo, Canada in 1997 and M.A.Sc. and Ph.D. degrees in electrical engineering from the University of Toronto, Canada in 1999 and 2003 respectively.

He is a Professor in the Department of Electrical and Computer Engineering, McMaster University (Hamilton, Ontario, Canada) and currently serves as the Associate Dean (Academic). During 2010-2011 he spent his research leave as Senior Member, Technical Staff in Advanced Technology for Research in Motion, Waterloo, Canada. His research interests are in the areas of free-space and optical wireless communications, digital communication algorithms, and electronic and photonic implementation of coding and communication algorithms. He is the author of the book *Wireless Optical Communication Systems* (New York:Springer, 2004).

Dr. Hranilovic is a licensed Professional Engineer in the Province of Ontario and was awarded the Government of Ontario Early Researcher Award in 2006. In 2016 the title of University Scholar was conferred upon him by McMaster University. He has served as an Associate Editor for the *Journal of Optical Communications and Networking* and an Editor for the *IEEE Transactions on Communications* in the area of Optical Wireless Communications.